

Hybrid Approach to High-Frequency Microfluidic Mixing

Xize Niu, Liyu Liu, Weijia Wen,^{*} and Ping Sheng

Department of Physics and Institute of Nano Science and Technology, The Hong Kong University of Science and Technology, Clear Water Bay, Kowloon, Hong Kong, China

(Received 1 March 2006; published 24 July 2006)

We report the experimental verification of the predicted chaotic mixing characteristics for a polydimethylsiloxane microfluidic chip, based on the mechanism of multistage cross-channel flows. While chaotic mixing can be achieved within short passage distances, there is an optimal side channel flow pulsation frequency beyond which the mixing becomes ineffective. Based on the physical understanding of a Poincaré section analysis, we propose the installation of passive flow baffles in the main microfluidic channel to facilitate high-frequency mixing. The combined hybrid approach enables chaotic mixing at enhanced frequency and reduced passage distance in two-dimensional flows.

DOI: [10.1103/PhysRevLett.97.044501](https://doi.org/10.1103/PhysRevLett.97.044501)

PACS numbers: 47.61.Ne, 47.51.+a, 47.85.L-

Mixing two or more streams of fluids is an important issue in various microfluidic devices. But the mixing process is not trivial in the microscale, owing to the dominance of the viscous effect and hence laminar flows. Passive mixers are designed to induce three-dimensional helical fluid motions from patterned structural asymmetries [1–4] that can fold the streams into highly nested thin slices, so as to facilitate local molecular interdiffusion. Active mixers differ from the passive type in that external energy is intentionally put into the system to help achieve chaotic mixing. A cross-stream active mixer [5–7] represents such a system in which the flow in the main microfluidic channel is perturbed by actively controlled side channel flows. To our knowledge, there has been no report of active chaotic mixer which can be integrated onto a lab chip, owing to the complexity of the control scheme and difficulty in microfabrications.

Figure 1(a) shows a schematic depiction of the active mixer chip design, consisting of a main flow channel (200 μm in width and 40 μm in depth) and 6 pairs of orthogonal side channels (4000 μm in length at each side of the main channel, the same size cross section as the main channel, each pair separated by 200 μm from its neighbors). The mixer was fabricated with polydimethylsiloxane (PDMS) using soft lithography techniques [8,9], actuated by electrorheological (ER) fluid valves possessing the giant electrorheological effect [10]. Briefly, the operation of the mixer chip relies on the perturbation of the main channel flow in the x direction by cross-stream side channel flows in the y direction. The side channel flows are driven by pressure changes in the ER fluid channel, through thin membranes at the bottom of the control bars located at the end of each side channel. The membranes also serve the function of separating the oil-based ER fluid from the experimental fluids (50% sucrose water and dye solution with measured viscosity of 0.013 kg/m s and the dye diffusion constant $D = 3.12 \times 10^{-11}$ m/s), avoiding any direct interference between the two. Figure 1(b) shows schematically the working principle of the ER valves.

Square-wave electrical voltage signals (0–800 V) are applied between the electrodes to close or open the ER fluid flows, connected to a high pressure source on one side and a low pressure source on the other, so that the membranes on the two sides of the main channel can be pushed and pulled alternately, leading to pulsating sinusoidal cross-stream flows in the 6 pairs of side channels. The mixing

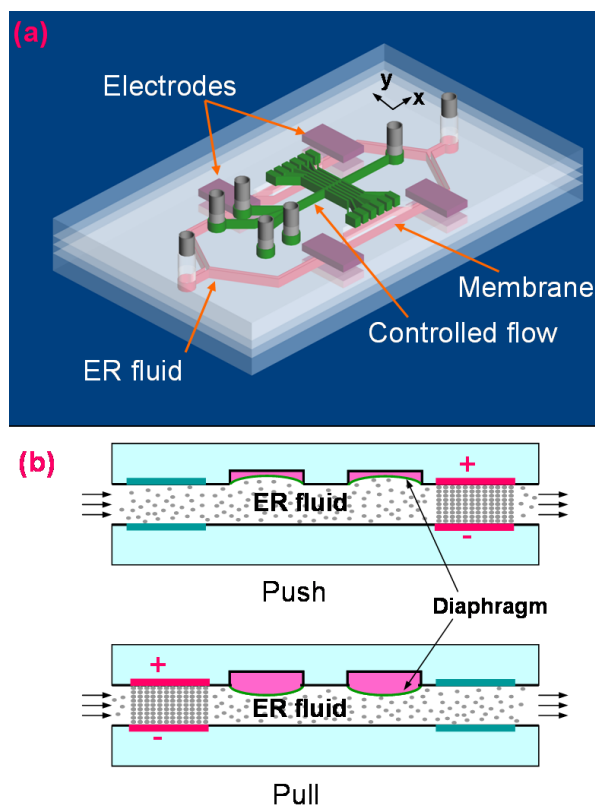


FIG. 1 (color online). (a) Schematic picture showing the PDMS active mixer design and construction. The overall chip size is 3 cm by 1.5 cm. (b) Schematic illustration showing the working principle for the push and pull ER valve, for one cross sectional area of ER fluid channel and control bars.

channel design is similar to that in Ref. [4] but with wider side channels and a different actuation strategy. The merits of ER fluid actuation are: (1) the perturbation frequency and amplitude can be digitally adjusted in chip to avoid time delays and complicated peripherals; only one pump (Masterflex© C/L currently used) is needed to circulate the ER fluid through the chip continuously, providing pressure and vacuum sources; (2) the giant ER effect assures that the ER control channel can modulate large shear stress, thereby supplying large perturbations; (3) such modulations can drive the membrane area as fast as 20 Hz or above due to the fast response of the ER fluid (in the milliseconds) and the rapid pressure buildup used in the design. Such a mixer can be readily integrated with a fast response microvalve or valve array or micropumps into a laboratory chip.

Mathematical description of the channel flows for mixing, first introduced by Volpert *et al.* [11], is the superposition of parabolic main channel flow $\dot{x} = U[1 - (2y/L)^2]$, and sinusoidal side channel flows $\dot{y} = v_p[1 - (2x/L)^2] \times \sin(\Omega t)$. In our mixer, the perturbation amplitude and frequency are the same for all side channels. The non-dimensionalized model can be written as

$$\dot{x} = \begin{cases} 1 - 4y^2 & \text{if } |y| < 1/2 \\ 0 & \text{if } |y| > 1/2 \end{cases} \quad (1a)$$

$$\dot{y} = \begin{cases} A_p[1 - 4(x - x_c)^2] \sin(\omega t) & \text{if } |x| < x_p + 1 \\ 0 & \text{if } |x| > x_p + 1 \end{cases}, \quad (1b)$$

where the length unit is the channel width L (200 μm in the present case), time unit is L/U , velocity unit is U , and the dimensionless angular frequency is given by $\omega = L\Omega/U$, and $x_c = 2\text{INT}[x/2] + 1$, where INT means taking the largest integer value smaller than the quantity inside the brackets. In addition, we also define a $U_0 = L/s$ (0.2 mm/s in the present case). Side channel perturbation amplitude $A_p = v_p/U$ and ω are the two control parameters which can be adjusted via ER valves.

It is seen that the model described by Eq. (1) involves nonlinear iterative mappings between x - and y -directional flows through time stepping. The trajectory of a fluid particle can thus have widely different behaviors depending on the magnitude of A_p and ω . We analyze these behaviors by using the Poincaré sections of the non-dimensionalized model, which can provide full mixing information of the system characterized with the parameter group $[U, v_p, \Omega]$. Scaling also dictates that the state with $[kU, kv_p, k\Omega]$ for any positive k on the Poincaré sections behaves the same as those with $[U, v_p, \Omega]$. Similarly, Lyapunov exponent (LE), the index of mixing intensity used in dynamical system theory, can be generalized directly from its definition,

$$\lambda = \lim_{t \rightarrow \infty} \lim_{d_0 \rightarrow 0} \frac{1}{t} \ln \frac{d(t)}{d_0} = \frac{U}{L} \lambda^*, \quad (2)$$

where λ^* is the LE of the normalized system (1), d_0 is the separation of the two fluid particles at $t = 0$, $d(t)$ is the separation at a later time t .

Figure 2 depicts, in color, the numerical results of the mean LE distribution on the $A_p - \omega$ plane for all of the fluid particles flowing into the main channel in one period of time. Here we have fixed $U = U_0$. The distribution indicates that there are areas of high LE and regions of low LE, with intermediate values in between. LE is small or close to zero in the partially chaotic regime; while in the fully chaotic regime most or all of the fluid particles have positive LEs, indicating ergodic character of the chaotic mixer. From Fig. 2, the LE distribution for any other value of $U = kU_0$ can be deduced from Eq. (2), i.e., $\lambda(kU_0, v_p, \Omega) = k\lambda^*(U_0, v_p/k, \Omega/k)$. The minimal mixing time needed, τ_{mix} , for fully chaotic mixing satisfies [12] $\tau_{\text{mix}} \propto \frac{1}{2\lambda} \ln \frac{\lambda L^2}{D}$. Hence the characteristic mixing time and length can be dramatically decreased for higher LE.

A series of experiments were carried out along the a - a' line in Fig. 2, to verify the theoretical predictions. The detailed experimental condition can be found in Ref. [9]. Figures 3(a)–3(c) show graphically the experimental results of fixing $\omega = 2\pi$, $U = U_0$, and increasing A_p from 0.5 [3(a)] to 4.0 [3(b)] to 7.2 [3(c)]. The flow direction in the main channel is indicated by the white arrow in Fig. 3(a). When $A_p = 0$, only static parabolic creeping flow exists in the main channel, with weakly attached Hele-Shaw flows at the intersection areas. The two streams of red and blue liquids flow separately, and molecular diffusion across the interface can be clearly observed in magnified scale. When A_p is increased (by increasing the electric field strength E applied to the ER valves), the system becomes partly chaotic [3(a)]. As A_p increases beyond 1, full mixing is achieved [3(b) and 3(c)]. To

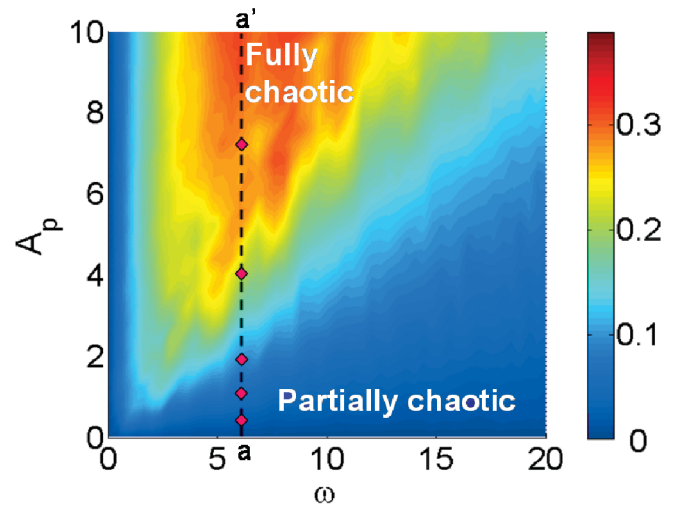


FIG. 2 (color). Mean Lyapunov exponent distribution in the A_p - ω parameter space for fluid particles fed into the main channel during one period of side channel pulsation.

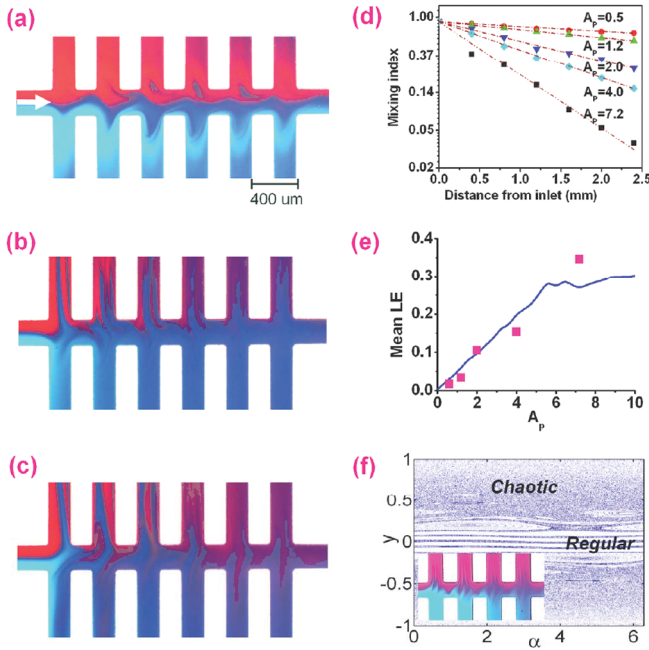


FIG. 3 (color). (a)–(c) Micrographs on mixing along the channel with different perturbation amplitude, $w = 2\pi$, $A_p = 0.5$, 4.0, and 7.2, respectively. (d) Mixing index vs channel length (from the beginning of the first side channel) for different A_p , $w = 2\pi$. The dotted lines are curve fitting of exponential decay of the mixing index. (e) The comparison between numerical and experimental LE values for different A_p . (f) Poincaré section of the mixer model for $U = U_0$, $A_p = 4$, $\omega = 13.5$. Inset to (f) shows a micrograph at the same parameters.

evaluate the mixing homogeneity along the main channel, we calculated the mixing index, M_i , by collecting on video frames the concentration of dyes in a pixel slice of the main channel right after each pairs of side channels, with the definition $M_i = \frac{1}{\bar{c}} \sqrt{\frac{\sum (c_j - \bar{c})^2}{N}}$, where \bar{c} is the mean concentration of the mixed dye solution, N is the total number of pixels, and the index i indicates the ordering of the side channel pairs, and j is the index for the pixels, $j = 1, \dots, N$. Because the movement of fluid elements in the channel is time dependent, all the video frames in one period of side channel pulsation were included in the evaluation. The decrease of M_i versus the distance from the inlet is given in Fig. 3(d), where the symbols are experimental data, and the lines are fitted to the exponential decay law. It is seen that the exponential law, expected from numerical simulation of the theoretical model, is well obeyed. The corresponding LEs for each case in Fig. 3(d) were collected [13] and compared with numerical results in Fig. 2, shown in Fig. 3(e). We find empirically that the theoretical Lyapunov exponent values correlates well with the same measure of mixing obtained from Fig. 3(d). It is concluded that chaotic mixing can be fully achieved in this ER-controlled microfluidic mixer chip. For $U > U_0$, the

control parameters A_p and ω would have to be increased proportionally according to the above analysis in order to achieve fully chaotic mixing.

Figure 2 clearly indicates the existence of an optimal ω range in the fully chaotic area, on the order of 5 to 8 (the values can vary with A_p), outside of which poor or no mixing can occur. That is, unless very large A_p is used, which would be incompatible with chip integration, frequencies higher than the optimal range are ineffective. Both to verify this prediction as well as to understand its underlying cause, we analyze the Poincaré section [3(f)] obtained from time stepping of (1) on the $y - \alpha$ plane [α being a transformation of time t by $\alpha = \text{mod}(\omega t, 2\pi)$], for $U = U_0$, $A_p = 4$, and $\omega = 13.5$ (seen to be located in the partially chaotic region in Fig. 2). It is seen that in the middle of the section, corresponding to fluid particles in the middle of the main channel, the Poincaré section has the shape of wavy continuous lines corresponding to Poiseuille flows with no mixing, generally denoted the Kolmogorov-Arnold-Moser (KAM) river. The inset to Fig. 3(f) shows a snapshot of the experiment carried out at the same parameters; the two streams are clearly not mixed, in agreement with the theoretical prediction. However, a closer inspection of Fig. 3(f) indicated the existence of randomly scattered dots, obtained from the projections of chaotic trajectories. These trajectories belong to fluid particles situated close to the channel walls, and their chaotic trajectories arise from repeated encounters with the geometric corners at the intersections of the main and side channels, which act as bifurcation points [6].

During the high-frequency oscillations in the y direction, the fluid-fluid interface would be stretched, but does not have enough time of travel to touch the corners. Hence if the interface lies in the KAM river as in Fig. 3(f), it cannot be cut into segments by the corners. The interface will hence experience spatiotemporal resonance in the channel, while retaining the interface integrity. Such phenomenon was indeed observed by Okkels and Tabeling [7].

The above understanding readily suggests a hybrid approach to more effective high-frequency microfluidic mixing, by adding baffles in the main channel, close to the interface line as shown in Fig. 4. The baffles would induce the interface line to encounter more bifurcation points during the high-frequency oscillations. In this approach the cross-stream perturbations from the side channels is a necessary element since without them the baffles would act as passive mixers, and it is well known that 2D flows (as in the present case) in passive mixers cannot induce chaotic mixing. This point is clearly demonstrated in Fig. 4(a), where the main channel flow with no side channel pulsations is shown to cause no mixing. When a small amplitude perturbation of $A_p = 0.5$ (0.1 mm/s) and $\omega = 20$ (20 rad/s) is added with $U = 0.2$ mm/s [4(b)], the interface is seen to be severely stretched and folded. Fully chaotic mixing [4(c)] is achieved after 2 pairs of side

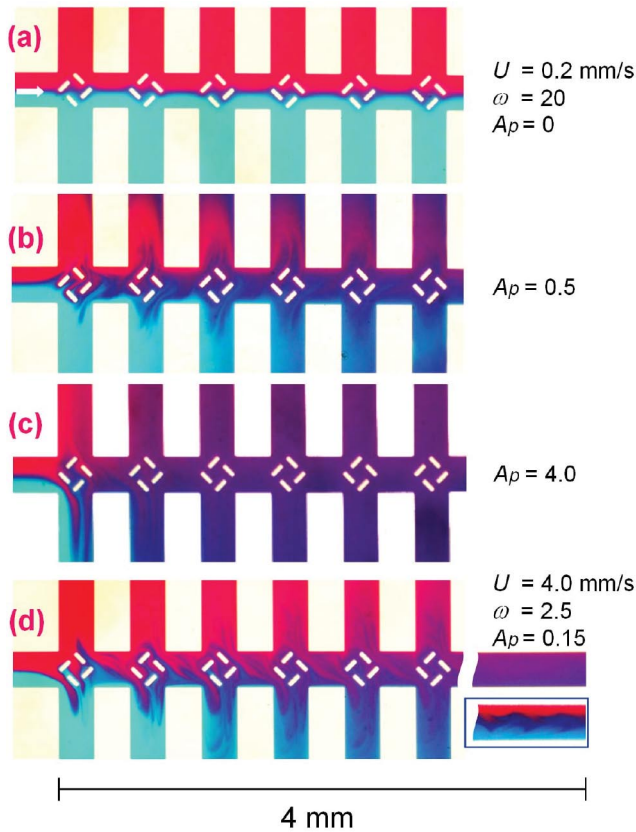


FIG. 4 (color). Micrographs on mixing along the baffled channel. Main channel flow speed $U = 0.2$ mm/s, $\omega = 20$ (20 rad/s); and $A_p = 0, 0.5$ (0.1 mm/s), and 4 (0.8 mm/s), respectively, for (a), (b), and (c). For (d), $U = 4$ mm/s, $\omega = 2.5$ (50 rad/s); $A_p = 0.15$ (0.6 mm/s). The downstream picture (2 mm from the last side channel pair) is also shown, indicating mixing has been completed. This is in contrast to the downstream picture of the main channel with the baffles removed (in box), in which only partial mixing is seen.

channels (0.6 mm in passage distance) when perturbation amplitude is increased to $A_p = 4$ (0.8 mm/s). Without baffles, such parameter will induce spatiotemporal resonances as analyzed above. Therefore KAM rivers were effectively eliminated in the hybrid approach.

For a high flow speed $U = 4$ mm/s, the residual time of liquid blobs in a 2 mm long mixing channel is noted to be ~ 0.5 s, implying a maximum molecular diffusion distance of $6 \mu\text{m}$ if relying on passive mixing only. But with side channel perturbations at $A_p = 0.15$ (0.6 mm/s) and $\omega = 2.5$ (50 rad/s), only few unmixed liquid blobs can be detected after 6 pairs of side channels [4(d)]. Most of the original $100 \mu\text{m}$ wide bulk liquid has been stretched and folded to 1 order of magnitude thinner, making molecular

diffusion much more effective. This can be seen in the downstream picture ~ 2 mm from the last side channel pair, at which point the molecular diffusion has completed the mixing process. Thus the hybrid approach has done its role in ~ 2 mm even at such high flow rate and frequency.

Not confined in the current ER fluid-driven mixer, such a hybrid approach can be readily used in a wide variety of 2D or 3D active mixers, e.g., piezoelectric, ac electrokinetic, or bubble-driven mixers that can achieve periodical perturbations to the main channel flows.

We acknowledge the support of Hong Kong RGC Grants No. 604205 and No. 604104. Xize Niu would like to thank Professor Yi-Kuen Lee.

*Email address: phwen@ust.hk

- [1] A. D. Stroock, S. K. W. Dertinger, A. Ajdari, I. Mezić, H. A. Stone, and G. M. Whitesides, *Science* **295**, 647 (2002).
- [2] S. Wiggins and J. M. Ottino, *Phil. Trans. R. Soc. A* **362**, 937 (2004).
- [3] C. Simonnet and A. Groisman, *Phys. Rev. Lett.* **94**, 134501 (2005).
- [4] R. H. Liu, M. A. Stremler, K. V. Sharp, M. G. Olsen, J. G. Santiago, R. J. Adrian, H. Aref, and D. J. Beebe, *J. Microelectromech. Syst.* **9**, 190 (2000).
- [5] F. Bottausci, I. Mezić, C. D. Meinhart, and C. Cardonne, *Phil. Trans. R. Soc. A* **362**, 1001 (2004).
- [6] X. Z. Niu and Y. K. Lee, *J. Micromech. Microeng.* **13**, 454 (2003).
- [7] F. Okkels and P. Tabeling, *Phys. Rev. Lett.* **92**, 038301 (2004).
- [8] Y. N. Xia and G. M. Whitesides, *Annu. Rev. Mater. Sci.* **28**, 153 (1998).
- [9] X. Z. Niu, L. Liu, W. Wen, and P. Sheng, *Appl. Phys. Lett.* **88**, 153508 (2006).
- [10] W. J. Wen, X. X. Huang, S. H. Yang, K. Q. Lu, and P. Sheng, *Nat. Mater.* **2**, 727 (2003).
- [11] M. Volpert, I. Mezić, C. D. Meinhart, and M. Dahleh, *Proceedings of the ASME Mechanical Engineering International Congress and Exposition, MEMS, Nashville, TN* (ASME, New York, 1999), p. 483.
- [12] F. Raynal and J. N. Gence, *Int. J. Heat Mass Transf.* **40**, 3267 (1997).
- [13] To estimate the Lyapunov exponents from the experimental data of mixing index, we first estimate the exponential decay of the mixing index versus the channel length from Fig. 3(d) by curve fitting, then the minimum mixing length, L_{mix} , needed in each case (until the mixing index below 0.1) is estimated according to such exponential decay tendency. Lyapunov exponent is calculated from the equation $L_{\text{mix}} = L^2 U / D \times e^{-2\lambda L_{\text{mix}} / U}$ [Ref. [6]].